Traveling-wave convection in a binary fluid mixture under high-frequency vertical vibrations

B. L. Smorodin,[1,*] B. I. Myznikova,[2] and S. M. Ishutov[1]

[1]*Department of Physics of Phase Transitions, Perm State University, 15 Bukirev Street, 614990 Perm, Russia*

[2]*Institute of Continuous Media Mechanics, Ural Branch of the Russian Academy of Sciences, 1 Academician Korolyov Street, 614013 Perm, Russia*

(Received 30 October 2013; published 7 May 2014)

The convective stability thresholds and nonlinear spatiotemporal evolution of convective rolls in a plane horizontal layer subject to steady gravity and high-frequency transversal vibration are numerically investigated considering a laterally periodic convective cell with rigid, impermeable horizontal boundaries. Simulations are performed for parameters adapted to laboratory experiments with an ethanol-water mixture with negative Soret coupling between temperature and concentration gradients. The characteristics of the wave and steady patterns are investigated depending on heat and vibration intensities. The weakly nonlinear traveling wave and modulated traveling wave are found as stable solutions within certain domains of parameters. Temporal Fourier decomposition is used together with other diagnostic tools to analyze the complex bifurcation and spatiotemporal properties that are caused by the interplay of the high-frequency vibrations, Soret induced gradients, and mixing of the fluid.

DOI: 10.1103/PhysRevE.89.053004 PACS number(s): 47.20.Ky, 47.55.P−, 47.54.−r

I. INTRODUCTION

Vibrations, alternating electric fields, and temperature modulation can efficiently affect the characteristics of technological processes. A classical example of the qualitative change in the response of a physical system placed in an alternating field is the Kapitza pendulum [1]. An alternating action can also considerably affect the stability and nonlinear dynamics of convective systems [2–4], which can be used to control hydrodynamics and heat and mass transfer in various technological devices.

Thermal vibrational convection is a set of phenomena associated with the appearance of regular flows in an inhomogeneous fluid under the action of vibration. An instability mechanism for such motion manifests itself even in microgravity [2–5]. In pure liquids the instability appears as a result of the forward bifurcation and evolution of monotonic disturbances. In binary mixtures with the negative separation ratio the lighter component migrates to the colder regions, thereby decreasing the density stratification in the conductive fluid state. Under these conditions the convection onset is associated with the backward Hopf bifurcation and the growth of the oscillatory perturbations. As a result, there is a great variety of spatiotemporal states in the binary-mixture convection, such as extended standing and traveling waves and the localized states [6–11]. The rich diversity of the patterns is determined by the evolution of the concentration field. Its redistribution, due to convection and thermal diffusion phenomena, affects the change of buoyant force acting on a unit volume of the mixture, and hence the velocity of convective flow.

The vibration force also affects the intensity of the global convective motion, and in combination with the buoyancy changes the convective velocity field. This leads to effects that are absent under static gravity conditions. For example, it is shown in Ref. [5] that the standing wave regime can be stabilized at some values of the amplitude and frequency of vibration.

The theory of convection in binary mixtures can be handled by means of the Boussinesq approximation taking into account dissipative processes of diffusion and thermal diffusion [12,13]. At high-frequency forcing, the period of vibrations is smaller than characteristic time scales for diffusive transport of momentum, heat, and concentration, and therefore it is reasonable to use the averaging approach for derivation of the governing equations of convection [14]. The amplitude and frequency of vibrations are combined into one nondimensional parameter referred to as the vibrational Rayleigh number, which is also called the Gershuni number [15].

The interrelation of convection and thermal diffusion in binary mixtures can be used as one of the control parameters in different technological processes, for example, the separation of fractions in the petrochemical industry, and many others, which motivate the investigation of thermovibrational convection excitation and nonlinear supercritical convective flow patterns in certain parameter ranges.

The stability of a horizontal binary-mixture layer, bounded by rigid impermeable plates and subjected to transversal high-frequency vibrations, has been considered in Ref. [16] taking into account also the impact of thermodiffusion.

The purpose of the present paper is to describe our results of numerical simulations of thermovibrational convection in binary liquid mixtures with the negative Soret coefficient (for instance, ethanol-water) valid in the case of high-frequency vibration. We found a stable, weakly nonlinear traveling-wave regime and a strongly nonlinear regime of modulated traveling wave (MTW). The theoretical explanation of the numerical results is given depending on parameter range.

The paper is organized as follows. In Sec. II we describe the situation under consideration, and introduce the mathematical model. Section III A contains the linear stability theory of the quasiequilibrium basic state with respect to small normal perturbations. The computational method and results of direct numerical simulations within the two-dimensional problem are presented in Sec. III B. The importance of transitions and dependencies observed is discussed in Sec. IV.

*bsmorodin@yandex.ru

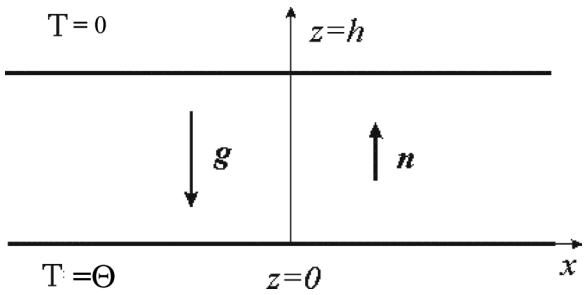

FIG. 1. Problem geometry and coordinate system.

II. FORMULATION OF THE PROBLEM

An infinite plane horizontal layer bounded by two parallel rigid plates is filled with a binary mixture of nonreacting constituents (for example, ethanol-water), and its boundaries are impermeable for the mixture components. The x axis of the Cartesian coordinate system is directed along the layer, while the z axis is normal to its boundaries (Fig. 1). Due to the thermal diffusion a concentration gradient is developed in the mixture, when a vertical temperature gradient is applied to the boundaries: $T(z=0)=\Theta$, $T(z=h)=0$.

The equation of state of the mixture can be written in the form

$$\rho = \bar{\rho}(1-\beta_T T-\beta_C C).$$

Here symbols T and C denote the deviations of the temperature and concentration from their mean values $\bar{T}$ and $\bar{C}$, respectively; β_T and β_C are the thermal and solutal expansion coefficients; $\bar{\rho}$ is the density of the mixture at certain mean values of temperature $\bar{T}$ and concentration $\bar{C}$. Assuming that C is the concentration of the light component, we obtain $\beta_C > 0$.

The layer is located in the static gravity field with the acceleration $\boldsymbol{g} = -g\boldsymbol{n}$ ($\boldsymbol{n}$ is an upward unit vector), and subjected to harmonic vibrations, transversal to the layer boundaries, with the amplitude b and the angular frequency Ω. We consider the limit of high-frequency (but below acoustic) vibrations with the period $T_v = 2\pi/\Omega$, which is much less than the time scales for diffusive transport of momentum, heat, and concentration across the layer:

$$T_v \ll \min\left[\frac{h^2}{\nu}, \frac{h^2}{\chi}, \frac{h^2}{D}\right].$$

Here ν is the kinematic viscosity, χ is the thermal diffusivity and D is the concentration diffusion constant of the mixture, respectively.

The governing equations for the mean parts of the velocity v, temperature T, concentration C, and additional variable w, which changes slowly with time, are obtained by means of the standard averaging procedure applied to the equations of the buoyancy convection within the Oberbeck-Boussinesq approximation [4,14]. Using the layer thickness h for the length, h^2/χ for the time, χ/h for the velocity, Θ for the temperature, $\beta_T\Theta/\beta_C$ for the concentration, and $\bar{\rho}\nu\chi/h^2$ for the pressure, one can write the averaged dimensionless equations of the thermovibrational convection in a binary mixture as follows:

$$\begin{aligned}
\frac{1}{\mathrm{Pr}}\frac{\partial v}{\partial t} + \frac{1}{\mathrm{Pr}}(v\nabla)v &= -\nabla p + \Delta v + \mathrm{Ra}(T+C)\mathbf{n} \\
&\quad + \mathrm{Gs}\,(w\nabla)\,[(T+C)\mathbf{n} - w], \\
\frac{\partial T}{\partial t} + (v\nabla)T &= \Delta T, \quad \mathrm{div}\, v = 0, \quad \mathrm{div}\, w = 0, \\
\mathrm{rot}\, w &= \nabla(T+C)\times\mathbf{n} = 0, \\
\frac{\partial C}{\partial t} + (v\nabla)C &= \mathrm{Le}\Delta(C-\psi T),
\end{aligned} \tag{1}$$

where p is the pressure, and the dimensionless parameters

$$\begin{aligned}
&\mathrm{Ra} = g\beta_T\Theta h^3/\nu\chi, \quad \mathrm{Gs} = (b\Omega\beta_T\Theta h)^2/2\nu\chi, \\
&\mathrm{Pr} = \nu/\chi, \quad \mathrm{Le} = D/\chi, \\
&\psi = -\kappa_T\beta_C/\bar{T}\beta_T = -\bar{C}(1-\bar{C})S_T\beta_C/\beta_T,
\end{aligned}$$

are the Rayleigh number, the Gershuni number, the Prandtl number, the Lewis number, and the separation ratio, respectively, while $\kappa_T = \bar{T}\bar{C}(1-\bar{C})S_T$ is the thermodiffusion coefficient and S_T is the Soret coefficient.

The equation of motion in Eq. (1) includes the additional vibrational force dependent on the temperature and the concentration inhomogeneities and on the slow variable w, which is actually the amplitude of pulsation velocity. In the equation of concentration we took into account the thermal diffusion effect, whose intensity is characterized by the separation ratio ψ. The sign of this parameter indicates the direction of the mass flux of the solute due to the thermal diffusion. We consider the case $\psi < 0$ (the so-called negative Soret coupling), when the light component migrates in the direction opposite to the temperature gradient.

The problem specified by the system of equations (1) has the conductive distributions of both temperature and solute concentration in a motionless liquid [16]:

$$v_0 = 0, \quad T_0 = 1-z, \quad \frac{dC_0}{dz} = -\psi, \quad w_0 = 0. \tag{2}$$

To solve numerically the problem of thermovibrational convection in the form of rolls with axes oriented along the y axis, two stream functions $\Psi(x,z,t)$ and $F(x,z,t)$, and the vorticity function $\varphi(x,z,t)$ are introduced, which are velocity related as follows:

$$\begin{aligned}
&v_x = \frac{\partial\Psi}{\partial z}, \quad v_z = -\frac{\partial\Psi}{\partial x}, \quad w_x = \frac{\partial F}{\partial z}, \\
&w_z = -\frac{\partial F}{\partial x}, \quad \varphi = (\mathrm{rot}\, v)_y.
\end{aligned} \tag{3}$$

The formulation of the problem in terms of the following five scalar fields (Ψ,φ,F,T,C) is written as follows:

$$\begin{aligned}
&\frac{1}{\mathrm{Pr}}\frac{\partial\varphi}{\partial t} + \frac{1}{\mathrm{Pr}}\left\{\frac{\partial\Psi}{\partial z}\frac{\partial\varphi}{\partial x} - \frac{\partial\Psi}{\partial x}\frac{\partial\varphi}{\partial z}\right\} = \Delta\varphi + \mathrm{Ra}\frac{\partial(T+C)}{\partial x} \\
&\quad + \mathrm{Gs}\left[\frac{\partial(T+C)}{\partial x}\frac{\partial^2 F}{\partial x\partial z} - \frac{\partial^2 F}{\partial x^2}\frac{\partial(T+C)}{\partial z}\right], \\
&\frac{\partial T}{\partial t} + \frac{\partial\Psi}{\partial z}\frac{\partial T}{\partial x} - \frac{\partial\Psi}{\partial x}\frac{\partial T}{\partial z} = \Delta T,
\end{aligned}$$

$$\frac{\partial C}{\partial t}+\left\{\frac{\partial \Psi}{\partial z}\frac{\partial C}{\partial x}-\frac{\partial \Psi}{\partial x}\frac{\partial C}{\partial z}\right\}=\mathrm{Le}\Delta(C-\psi T),$$
$$\varphi=-\Delta\Psi,\quad \Delta F=\frac{\partial(T+C)}{\partial x}. \tag{4}$$

These equations are supplemented with boundary conditions,

$$\begin{aligned} z=0:&\quad \Psi=0,\quad \frac{\partial \Psi}{\partial z}=0,\quad F=0,\\ T=1,&\quad \frac{\partial C}{\partial z}-\psi\frac{\partial T}{\partial z}=0,\\ z=1:&\quad \Psi=0,\quad \frac{\partial \Psi}{\partial z}=0,\quad F=0,\\ T=0,&\quad \frac{\partial C}{\partial z}-\psi\frac{\partial T}{\partial z}=0, \end{aligned} \tag{5}$$

corresponding to no-slip, impermeable for solute, and isothermal horizontal plates, while lateral boundaries of the computational domain are treated as periodic. Therefore all the fields $\mathcal{F}\equiv\{\Psi,\varphi,F,T,C\}$ in the x direction are set to periodic:

$$\mathcal{F}(x,z,t)=\mathcal{F}(x+L,z,t). \tag{6}$$

In the present paper, we employ the set of parameters that is relevant for molecular liquid mixtures: the Lewis number $\mathrm{Le}=0.01$, the Prandtl number $\mathrm{Pr}=10$, and two values of negative separation ratio, $\psi=-0.25$, $\psi=-0.4$. This set of parameters characterizes the ethanol-water mixture [9,11,17].

III. NUMERICAL RESULTS

A. Linear stability analysis

First we briefly discuss the behavior of small disturbances of the basic state (2). Let us consider small normal disturbances of the conductive state (2) taken as

$$\{\Psi,T,\xi,F\}=\exp(\lambda t+ikx)\{\Psi(t,z),\,\theta(t,z),\,\xi(t,z),\,f(t,z)\}, \tag{7}$$

where $\xi=C-\psi T$ is the new variable, λ is the growth rate of the disturbances, and k is the wave number.

After linearization one can obtain the following spectral boundary value problem for small normal disturbances:

$$\begin{aligned} \frac{\lambda}{\mathrm{Pr}}\left(\frac{d^2}{dz^2}-k^2\right)\Psi&=\left(\frac{d^2}{dz^2}-k^2\right)^2\Psi+ik\mathrm{Ra}[(1+\psi)\theta+\xi]\\ &\quad+(1+\psi)k^2\mathrm{Gs}f,\\ \lambda\theta+ik\Psi&=\left(\frac{d^2}{dz^2}-k^2\right)\theta. \end{aligned} \tag{8}$$

$$\begin{aligned} \lambda\xi+ik\psi\Psi&=\mathrm{Le}\left(\frac{d^2}{dz^2}-k^2\right)\xi-\psi\left(\frac{d^2}{dz^2}-k^2\right)\theta,\\ \left(\frac{d^2}{dz^2}-k^2\right)f&=ik\left[\theta(1+\psi)+\xi\right],\\ z=0,1:&\quad \Psi=0,\quad \frac{\partial \Psi}{\partial z}=0,\\ f=0,&\quad \theta=0,\quad \frac{\partial \xi}{\partial z}=0. \end{aligned} \tag{9}$$

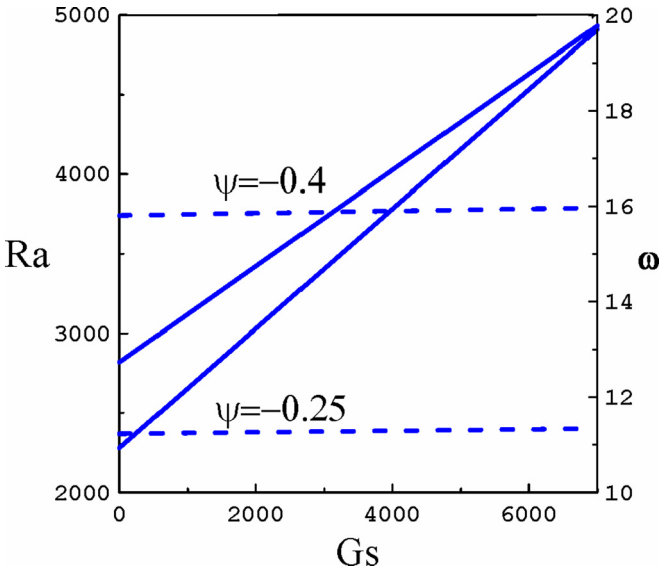

FIG. 2. (Color online) Critical values of the Rayleigh number Ra (solid lines) and frequency of neutral disturbances ω (dashed lines) versus the Gershuni number Gs for two values of separation ratio $\psi=-0.25$ and $\psi=-0.4$. The other parameters are $\mathrm{Le}=0.01$, $\mathrm{Pr}=10$.

It is known that when a horizontal binary-mixture layer with negative Soret coupling is heated from below, the long-wave instability mode does not exist, and instability is connected with the oscillatory disturbances with finite k [16]. We perform the linear stability analysis of the basic state with respect to disturbances with an arbitrary wave number by solving the spectral-amplitude problem (8) and (9). The numerical procedure is based on the shooting (sequential) method with the orthogonalization scheme for integration [18].

In the absence of vibration the critical wave number is $k\approx\pi$. According to the numerical results obtained within the range $0<\mathrm{Gs}<5200$ of the Gershuni number values, the decrease in the critical wave number does not exceed 25%, so in the further nonlinear simulations (see Sec. III B) we use the convective cell of length $L=2$ corresponding to the wave number $k\approx\pi$ in order to compare the heat and mass transfer due to thermovibrational convection with the convection of a binary mixture under the steady gravity.

In Fig. 2 the dependencies of the Rayleigh number and the oscillation frequency are presented versus the Gershuni number for neutral disturbances at two values of the separation ratio, $\psi=-0.25$ and $\psi=-0.40$. It can be seen that the increase in the intensity of vertical vibrations (or the Gershuni number Gs) stabilizes the quasiequilibrium state with raising an instability boundary almost linearly. The neutral oscillation frequency remains practically constant. The growth of absolute value of thermodiffusion parameter corresponding to the greater stratification of the mixture in the quasiequilibrium state causes an upward shift of the stability boundary and characteristic values of the oscillation frequency towards the increase. As the Gs grows, the difference of computed thresholds for two values of separation ratio ($\psi=-0.25$ and $\psi=-0.40$) decreases. Such behavior of the critical Rayleigh number and oscillation frequency may be explained

by analyzing the properties of (8) and (9). The field f is well represented by the first spatial harmonic in the horizontal position and vertical coordinate: $f = f_0 \exp(i\,kx)\sin(\pi z)$. The numerical results [see Sec. III B, Fig. 4(b)] support this assertion. Therefore the variable f can be excluded from Eqs. (8) and (9). Indeed, since

$$\left(\frac{d^2}{dz^2} - k^2\right) f = -(\pi^2 + k^2) f, \quad f = -\frac{i,k[\theta(1+\psi)+\xi]}{(\pi^2+k^2)},$$

then Eq. (8) takes the form

$$\frac{\lambda}{\mathrm{Pr}}\left(\frac{d^2}{dz^2} - k^2\right)\Psi = \left(\frac{d^2}{dz^2} - k^2\right)^2 \Psi + ik\left[\mathrm{Ra}_0 - \frac{(1+\psi)k^2\mathrm{Gs}}{(\pi^2+k^2)}\right] \times [(1+\psi)\theta + \xi], \tag{10a}$$

$$\lambda\theta + ik\Psi = \left(\frac{d^2}{dz^2} - k^2\right)\theta, \tag{10b}$$

$$\lambda\xi + ik\psi\Psi = \mathrm{Le}\left(\frac{d^2}{dz^2} - k^2\right)\xi - \psi\left(\frac{d^2}{dz^2} - k^2\right)\theta, \tag{10c}$$

where Ra_0 is the Rayleigh number in the absence of vibrations.

The system of equations describing convection thresholds under the high-frequency vibrations differs from the problem of binary-mixture convection under static gravity conditions only in the coefficient at the last term of the momentum equation (10a):

$$\mathrm{Ra(Gs)} = \mathrm{Ra} - \frac{(1+\psi)k^2\mathrm{Gs}}{(\pi^2+k^2)} \to \mathrm{Ra}_0. \tag{11}$$

This coefficient describes the change (namely, reduction) of the fluid buoyancy under vibrations with respect to the steady case of Ra_0. Therefore in the presence of vibration *ceteris paribus* the instability occurs under more intense heating.

The results of numerical simulations (see Fig. 2) are in good agreement with the analytical predictions for Ra(Gs). Moreover, for the long-wave mode ($k = 0$) Eq. (12) leads to the well-known result [16]

$$\mathrm{Ra(Gs)} = \mathrm{Ra}_0 = \frac{720\mathrm{Le}}{\psi}.$$

In the case of transversal vibrations the critical Rayleigh number in the long-wave limit does not depend on the Gershuni number Gs.

B. The nonlinear evolution of convective patterns

To obtain approximate solutions of the boundary value problem (4) and (5) the finite-difference technique is applied to a set of discrete points, uniformly spaced within the computational domain with respect to each independent variable. The parabolic equations are solved using central differences for the spatial derivatives and forward difference for time derivatives. This is a finite-difference method of second order. The elliptic equations for the stream functions were worked out by means of an iterative method of successive over-relaxation at each time step. Typically, a regime of steady-state, finite-amplitude convective oscillations obtained at a particular set of parameters was used as the initial condition for a run at a different set of parameters. The calculations were executed on a mesh of 42×21 nodes. Further refining the mesh did not have any significant effect on characteristics of the convective regimes.

We monitor the time evolution of the maximum of the stream function Ψ field in the x-z cross section perpendicular to the roll axes,

$$\Psi_{\max}(t) = \max_{x,z}[\Psi(x_i, z_j, t_k)], \tag{12}$$

as well as the local time evolution of Ψ at a fixed position ($x = L/4$, $z = 1/2$):

$$\Psi_l(t) = \Psi(x = L/4, z = 1/2, t). \tag{13}$$

To elucidate the spatiotemporal complexity of the convective behavior and transitions among various regimes we have also studied lateral Fourier decompositions [11],

$$\mathcal{F}(x,t) = \mathcal{F}_0(x,t) + \sum_{n=1}^{\infty} \mathcal{F}_n(t) e^{inkx} \tag{14}$$

of the fields at the midheight position, $z = 1/2$, which were found highly representative for the other z values. Here $\mathcal{F}_n(t)$ is the amplitude of the nth spatial harmonic.

To compare the numerical results obtained in this way with the well-known experimental, analytical, and numerical results of other authors, the reduced Rayleigh number $r = \mathrm{Ra}/\mathrm{Ra}_c$ is used, i.e., Ra is scaled by Ra_c, where $\mathrm{Ra}_c = 1686$ is the critical Rayleigh number for the onset of convection in homogeneous liquid obtained by means of our numerical code.

We are concerned with the properties of the convective system at different values of the Gershuni number. Let us consider first rather small Gs values at which the bifurcation diagram, presented in Fig. 3, does not qualitatively change compared to the no vibration case. It illustrates the maximum

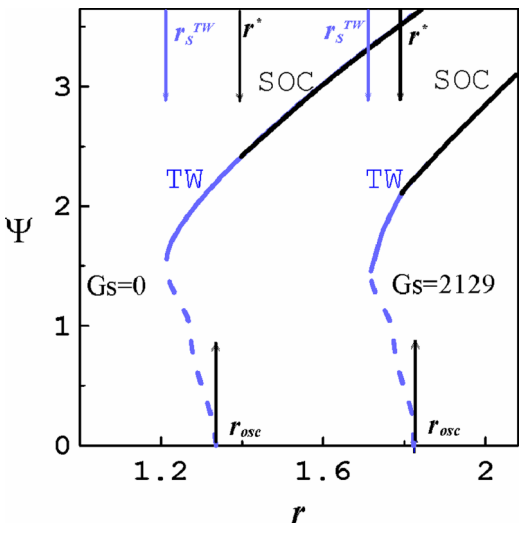

FIG. 3. (Color online) Bifurcation map of the traveling-wave (TW) solution and steady overturning convection (SOC) at the Gershuni numbers Gs = 0; 2129. Solid (or dashed) lines correspond to stable (or unstable) regimes.

of the stream function Ψ in the traveling-wave (TW) regime depending on the reduced Rayleigh number r at given values of the Gershuni number, $\mathrm{Gs} = 0$ and $\mathrm{Gs} = 2129$. When the heating intensity increases quasistatically, the onset of convection occurs via a Hopf bifurcation at the reduced Rayleigh number value $r_{\mathrm{osc}}(\mathrm{Gs})$ and is characterized by the Hopf frequency $\omega_H = 11.25$, which does not depend on the Gershuni number. The two-dimensional right and left traveling-wave solutions bifurcate backward out of the conductive state at $r_{\mathrm{osc}}(\mathrm{Gs})$, which is in good agreement with the predictions of the linear stability theory (see Sec. III A). The waves gain stability via a saddle-node bifurcation at the value of reduced Rayleigh number $r_S^{\mathrm{TW}}(\mathrm{Gs})$: $r_S^{\mathrm{TW}}(0) = 1.081$ and $r_S^{\mathrm{TW}}(2129) = 1.717$. The oscillation frequency and maximum of the stream function Ψ in saddle-node point does not depend on the Gershuni number: $\omega_S^{\mathrm{TW}}(0) = \omega_S^{\mathrm{TW}}(2129) = 3.25$, $\Psi_{\max}(\mathrm{Gs} = 0) = \Psi_{\max}(\mathrm{Gs} = 2129) = 1.46$.

Within the interval $r_S^{\mathrm{TW}} < r < r_{\mathrm{osc}}$ both stable TW regimes (solid lines in Fig. 3) and also unstable ones (dashed lines) exist. As under steady gravity conditions [11], the concentration fields of these two flow patterns are drastically different: The concentration field is strongly nonlinear in the stable regime, while it is weakly nonlinear when the traveling wave is unstable.

Within the range $r < r_S^{\mathrm{TW}}$ the binary-mixture convection decays and the system relaxes to the conductive state. The branch of stable TWs ends at the value of reduced Rayleigh number $r^*(\mathrm{Gs})$: $r^*(0) = 1.364$, $r^*(2129) = 1.794$, and the stationary overturning convection (SOC) solution is formed. Thus, the highly developed, nonlinear traveling-wave convection is stable within the interval of the reduced Rayleigh numbers $r_S^{\mathrm{TW}} < r < r^*$. Bifurcation diagrams constructed at different Gs values look similar; however, the growth of the Gershuni number leads to an increase in the critical values of the reduced Rayleigh numbers r_S^{TW}, r_{osc}, r^*. It worth pointing out that in the absence of vibrations the inequality $r_{\mathrm{osc}} < r^*$ is true. This peculiarity is also kept in the presence of transversal vibrations. It is necessary to note that all solutions are characterized by the additional field of stream function F, whose amplitude f is well described by the first spatial harmonic. It can be seen in Fig. 4 that the amplitude of this field is much less than the amplitude of stream function Ψ.

At rather high intensity of vibration ($\mathrm{Gs} > 4800$) the form of the bifurcation diagram changes. For instance, the bifurcation diagram presented in Fig. 5 corresponds to $\mathrm{Gs} = 5000$. The important unexpected fact is the behavior of the weakly nonlinear traveling-wave mode (TW-WN): It is stable in a certain range of the reduced Rayleigh number. The TW-WN solutions are characterized by large values of the phase velocity and therefore large values of the oscillation frequency observed in the fixed point inside the convective cell. The oscillation frequency at $r = 2.441$ (point B in Fig. 5) is relatively large and equals $\omega = 8.09$ that constitutes 70% of the Hopf one, $\omega_H = 11.25$, and is greater than ω_S^{TW}. The maximum stream function value $\Psi_{\max}$ in this regime does not depend on time. It is important to stress that in the absence of vibrations this convective pattern is unstable [11]. As in the case of the Kapitza pendulum [1] the high-frequency vibration modified some fundamental properties of the mechanical system, and an unstable regime may become stable.

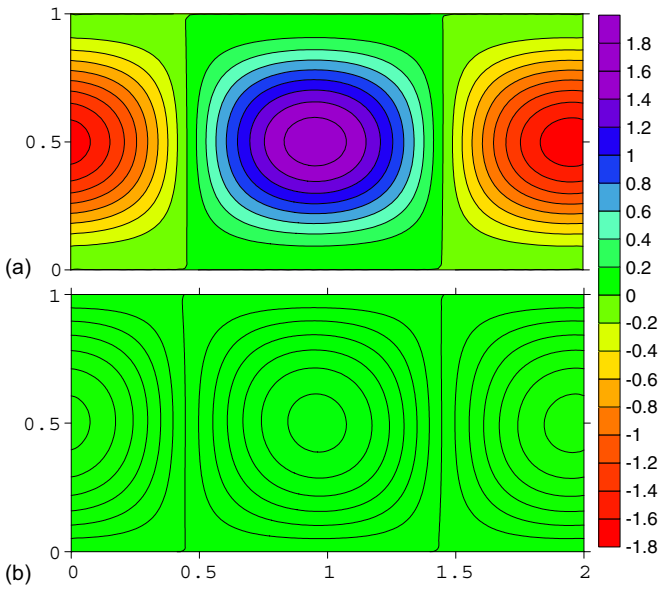

FIG. 4. (Color online) Snapshots of the stream functions fields in the convective cell at $\mathrm{Gs} = 2129$, $r = 1.75$: (a) $\Psi(x,z)$ and (b) $f(x,z)$.

The growth of the reduced Rayleigh number gives rise to a *stable regime* of modulated traveling wave (MTW), which is found within the parameter range $r_1 < r_{\mathrm{MTW}} < r_2$ shown in Fig. 5. Within the range $\boldsymbol{r}_{\mathrm{MTW}}$ the maximum over the domain value of the stream function $\Psi_{\max}(t)$ oscillates between upper $\Psi_1(r)$ and lower $\Psi_2(r)$ limits and therefore the amplitude of TW is modulated. The bifurcation diagram contains two dependencies, $\Psi_1(r)$ and $\Psi_2(r)$. Within the interval $r_1 < r_{\mathrm{MTW}} < r_2$ the growth of r leads to deepening the modulation and increasing the difference $\Psi_1(r) - \Psi_2(r)$. At $r = r_2$ the MTW mode becomes unstable and it is succeeded

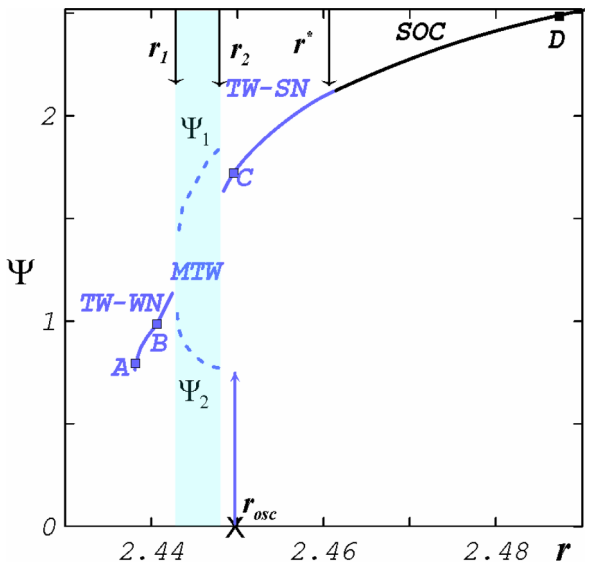

FIG. 5. (Color online) Bifurcation diagram of laterally extended convective states with the wave number $k = \pi$ in the binary liquid-mixture layer, as functions of the reduced Rayleigh number r, at $\mathrm{Gs} = 5000$, $\psi = -0.25$, $\mathrm{Le} = 0.01$, $\mathrm{Pr} = 10$.

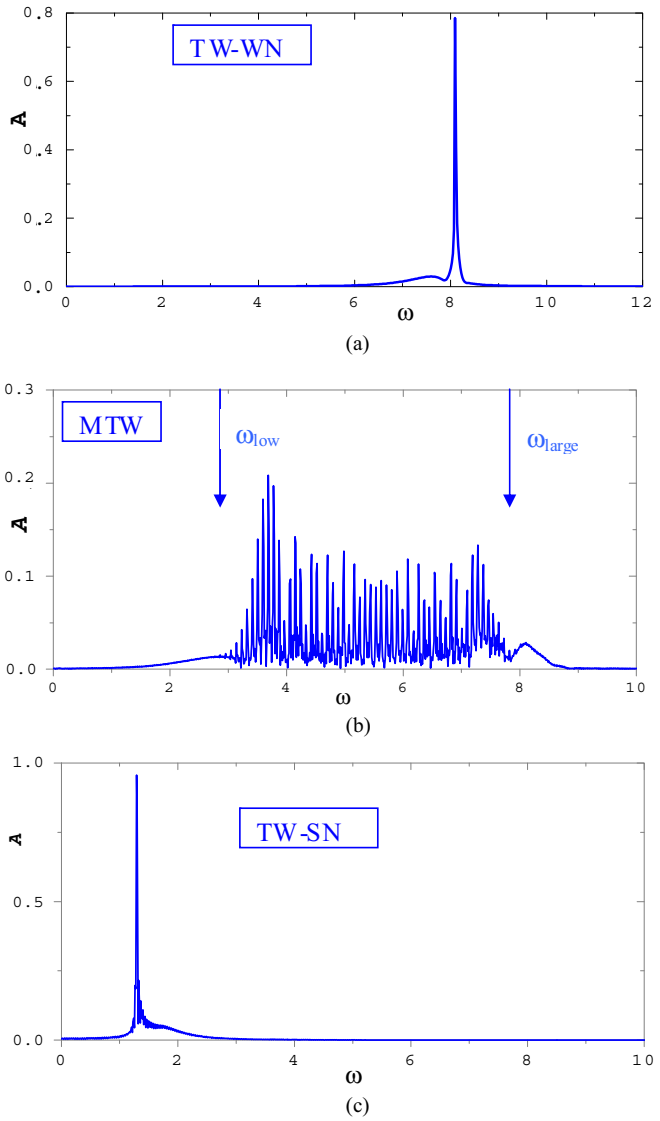

FIG. 6. (Color online) Amplitude A of the Fourier spectrum of $\Psi_l = \Psi(x = 0, z = 1/2, t)$ in arbitrary units versus frequency ω at Gs = 5000: (a) The weakly nonlinear traveling-wave regime TW-WN at $r = 2.441$; (b) the modulated traveling-wave regime at $r = 2.444$; (c) the strongly nonlinear traveling-wave regime at $r = 2.450$.

by a strongly nonlinear traveling-wave mode (TW-SN) with the concentration field revealing a plurality of higher spatial harmonics. Further growth of the reduced Rayleigh number results in decrease in phase velocity of the TW up to zero, and at $r > r^*$ the SOC pattern is ascertained (Fig. 5, point D).

Figure 6 illustrates the result of the Fourier transformation of the stream function $\Psi_l(t) = \Psi(x = L/4, z = 1/2, t)$ for different convective solutions. In the weakly nonlinear traveling-wave regime TW-WN [Fig. 6(a), $r = 2.441$] the Fourier spectrum of the stream function contains one main contribution. This solution is characterized by the large value of oscillation frequency $\omega = 8.09$ and therefore the phase velocity of traveling wave $v_{\rm ph} = \omega/k$. The Fourier spectrum in the modulated traveling-wave regime [Fig. 6(b), $r = 2.444$] contains the wide frequency interval $\Delta\omega = \omega_{\rm large} - \omega_{\rm low}$. The large frequency in this solution is the same as the oscillation

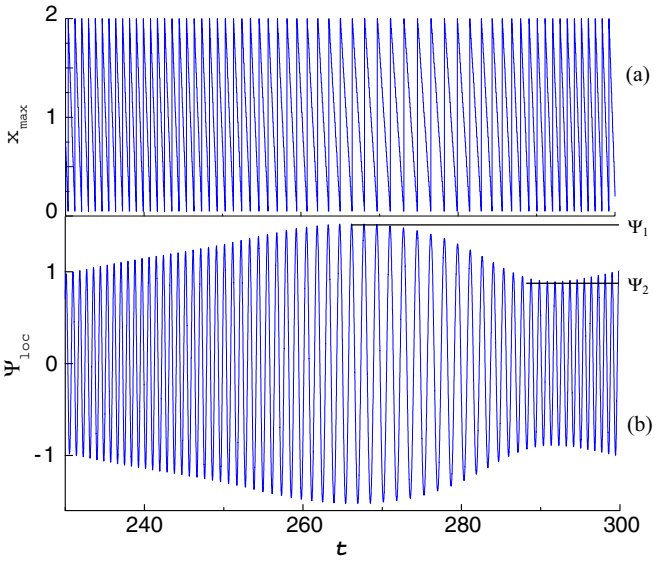

FIG. 7. (Color online) Time dependencies in the modulated traveling-wave regime at $r = 2.444$, Gs = 5000: (a) The horizontal coordinate of maximum stream function value $x_{\rm max}(t) = x[\Psi_{\rm max}(t)]$ and (b) the stream function value at the fixed position $\Psi_l = \Psi(x = L/4, z = 1/2, t)$.

frequency of the weakly nonlinear traveling-wave regime. The phase velocity of TW-SN solution is much less than that of a weakly nonlinear traveling wave, and in the Fourier spectrum only the low frequency, $\omega_{\rm low}$, survives [see Fig. 6(c), $r = 2.450$]. This frequency is approximately six times smaller than that in the TW-WN mode.

In the case of TW solution the horizontal coordinate $x_{\rm max}$ of the $\Psi_{\rm max}$ position moves through the computational domain between its lateral boundaries. The phase velocity of the traveling wave is determined by the slope of this line. It can be seen in Fig. 7 that both phase and amplitude modulations are present in MTW solution because both the phase velocity [Fig. 7(a)] and the maximum stream function value [Fig. 7(b)] change with time. The highest phase velocity values correspond to the minimum stream function values and therefore weak convective mixing. The growth of the stream function reflects the increasing convective mixing and reduces the phase velocity. The period of modulation is at least one order of magnitude greater than the period of its traveling-wave oscillations.

The concentration fields for the different convective solutions are shown in Fig. 8 by four snapshots of C in the x-z plane. On the left end point of the TW-WN range [Fig. 8(a), $r = 2.438$, point A in the bifurcation diagram] the concentration field is determined by the first spatial harmonic of the wave, as the stream functions and the temperature fields are. Within the TW-WN parameter range the growth of r changes the flow properties: Some spatial anharmonicity manifests itself in the concentration field [Fig. 8(b), $r = 2.441$, point B in the bifurcation diagram]. The strongly nonlinear TW mode has the large concentration gradients in narrow boundary layers between the convective rolls and near the horizontal plates [Fig. 8(c), $r = 2.450$, point C in the bifurcation diagram]. In SOC solution [Fig. 8(d), $r = 2.488$, point D in the

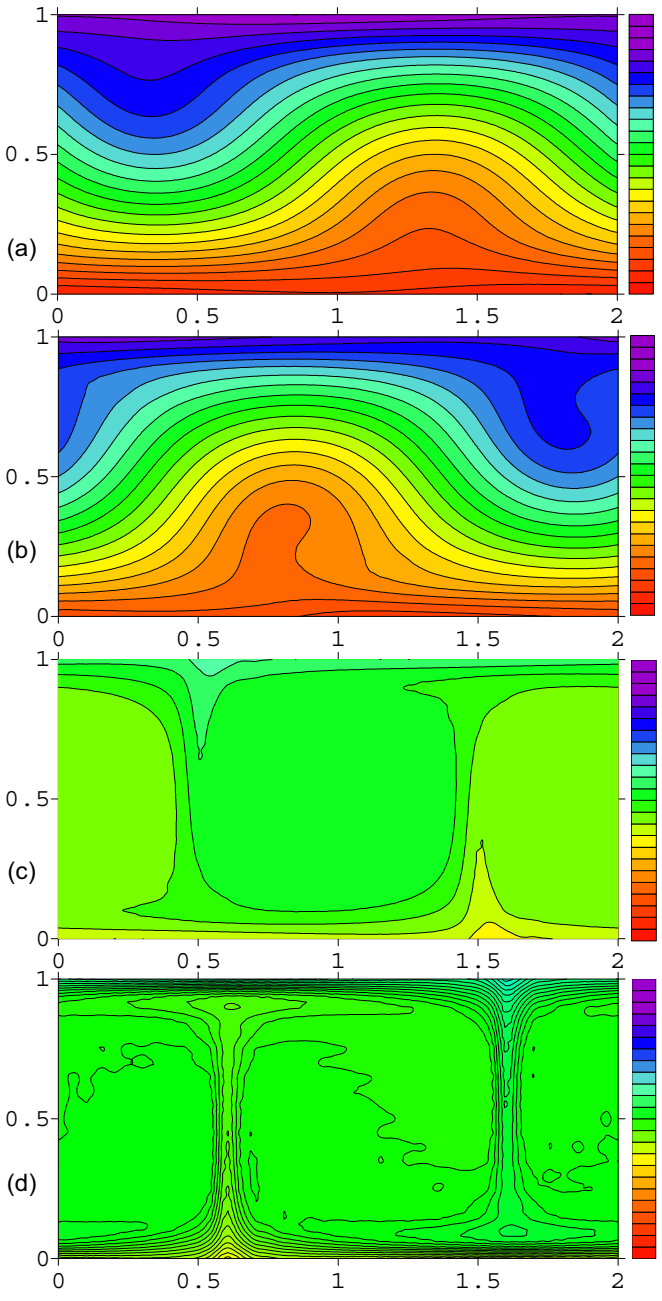

FIG. 8. (Color online) The snapshots of the concentration field for the weakly nonlinear traveling-wave regime WN-TW (a) $r = 2.438$, (b) $r = 2.441$, (c) strongly nonlinear traveling-wave regime TW-SN at $r = 2.450$, and (d) SOC regime at $r = 2.488$. The vertical color bars show the coding conductive state with C_{cond} varying linearly from -0.125 at the bottom to 0.125 at the top. Gs $= 5000$, $\psi = -0.25$, Le $= 0.01$, Pr $= 10$.

bifurcation diagram] the concentration field demonstrates the mirror symmetry between oppositely turning vortices, and the advective mixing is much more intensive in comparison with TW regimes. The concentration field in SOC solution looks like that in the absence of vibration [10,11].

Figure 9 represents the stability diagram of the convection modes in the parameter plane $\{r, \text{Gs}\}$. It shows that the growth of vibration intensity leads to an increase in the characteristic

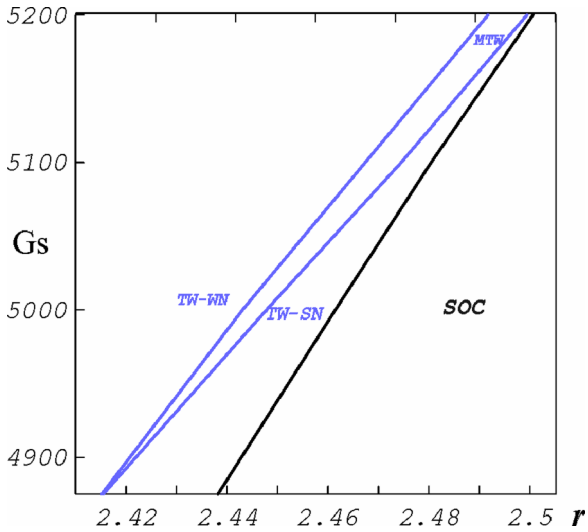

FIG. 9. (Color online) Map of regimes on the plane of parameters $\{r, \text{Gs}\}$: weakly nonlinear traveling wave TW-WN, modulated traveling wave MTW, strongly nonlinear traveling wave TW-SN, steady overturning convection SOC.

values of the critical parameter r^*. In addition to that, the extension of the r_{MTW} interval is observed in which the modulated traveling-wave flow pattern is stable.

Let us estimate the numerical values of physical parameters and characteristics of vibrations which might be useful to experimental testing. To achieve the typical value of the Gershuni number Gs ≈ 5100 and the Rayleigh number $\text{Ra} = 1686 \times r = 1686 \times 2.47 \approx 4160$, which belong to the region of MTW (see Fig. 9), we take the 8 wt% solution of ethanol in water at the mean temperature 28 °C. For this solution the physical parameters are as follows: $\beta_T = 2.8 \times 10^{-4}\ \text{K}^{-1}$, $\nu \approx 1.14 \times 10^{-6}\ \text{m/c}^2$, $\chi \approx 1.14 \times 10^{-7}\ \text{m/c}^2$ [9,17]. Using the amplitude $b = 79$ mm and frequency of vibration $f = 12$ Hz [16], depth of the layer $h = 3$ mm and temperature difference $\Theta = 7.3$ K, one can obtain required values of the Rayleigh number $\text{Ra} = \frac{g\beta_T \Theta h^3}{\nu\chi} = \frac{9.8(2.8\times10^{-4})7.3(3\times10^{-3})^3}{(1.14\times10^{-6})(1.14\times10^{-7})} \approx 4160$ and the Gershuni number $\text{Gs} = \frac{(b\Omega\beta_T\Theta h)^2}{2\nu\chi} = \frac{[(7.9\times10^{-2})6.28\times12(2.8\times10^{-4})7.3(3\times10^{-3})]^2}{2(1.14\times10^{-6})(1.14\times10^{-7})} \approx 5100.$

IV. CONCLUSION

The influence of high-frequency transversal vibrations on the convective instability and pattern formation in a binary mixture is investigated in the horizontal layer heated from below. Finite-difference numerical simulations were carried out for parameters adapted to experiments that use ethanol-water mixtures with negative Soret coupling. Various visualization tools were used to analyze the complex spatiotemporal properties of nonlinear response to high-frequency vibrations.

It is shown that an increase of the Gershuni number leads to an increase of the critical control parameters: reduced Rayleigh numbers r_S^{TW}, r_{osc}, r^*. The nonlinear convective patterns are found depending on the Rayleigh and Gershuni numbers:

weakly and strongly nonlinear TW, modulated TW, and SOC state. It is demonstrated that the unstable weakly nonlinear TW regime can be stabilized by means of high-frequency vibrations. This TW solution has high phase velocity. The *thermovibrational convection regime* of amplitude and phase modulated traveling wave (MTW) is found and theoretically analyzed. The contour plots of the stream function and concentration fields represent specific features of investigated convective flows. Our results are summarized in bifurcation diagrams displaying scenarios of possible transitions, as well as the stability map where the observed thermovibrational convection flow patterns are shown.

ACKNOWLEDGMENTS

The authors acknowledge the referees whose comments helped make the presentation of the material more straightforward. This work was partially supported by a grant provided by the Russian Foundation for Basic Research (Projects No. 13-01-96010 and No.14-01-96027).

[1] P. L. Kapitza, Zh. Eksp. Teor. Fiz. **21**, 588 (1951).
[2] G. Z. Gershuni and E. M. Zhukhovitskii, Dokl. Akad. Nauk SSSR **249**(3), 580 (1979).
[3] G. Z. Gershuni, I. O Keller, and B. L. Smorodin, Dokl. Akad. Nauk **348**(2), 194 (1996).
[4] G. Z. Gershuni and D. V. Lyubimov, *Thermal Vibrational Convection* (John Wiley & Sons, New York, 1997).
[5] B. L. Smorodin, B. I. Myznikova, and J. C. Legros, Phys. Fluids **20**, 094102 (2008).
[6] B. L. Smorodin and M. Lücke, Phys. Rev. E **79**, 026315 (2009).
[7] E. Moses, J. Fineberg, and V. Steinberg, Phys. Rev. A **35**, 2757(R) (1987).
[8] J. J. Niemela, G. Ahlers, and D. S. Cannell, Phys. Rev. Lett. **64**, 1365 (1990).
[9] D. Bensimon, P. Kolodner, C. M. Surko, H. Williams, and V. Croquette, J. Fluid Mech. **217**, 441 (1990).
[10] C. Fütterer and M. Lücke, Phys. Rev. E **65**, 036315 (2002).
[11] D. Jung, P. Matura, and M. Lücke, Eur. Phys. J. E **15**, 293 (2004).
[12] J. K. Platten and J. C. Legros, *Convection in Liquids* (Springer-Verlag, Berlin, Heidelberg, 1984).
[13] L. D. Landau and E. M. Lifschitz, *Course of Theoretical Physics*, Vol. 6 (Pergamon Press, Oxford, 1993).
[14] S. M. Zen'kovskaya and I. B. Simonenko, Izv. Akad. Nauk SSSR, Mekh. Zhidk. Gaza **5**, 51 (1966).
[15] A. Mialdun, I. I. Ryzhkov, D. E. Melnikov, and V. Shevtsova, Phys. Rev. Lett. **101**, 084501 (2008).
[16] G. Z. Gershuni, A. K. Kolesnikov, J.-C. Legros, and B. I. Myznikova, Int. J. Heat Mass Transfer **42**, 547 (1999).
[17] P. Kolodner, H. L. Williams, and C. Moe, J. Chem. Phys. **88**, 6512 (1988).
[18] U. M. Ascher, R. M. M. Mattheij, and R. D. Russell, in *Numerical Solution of Boundary Value Problems for Ordinary Differential Equations*, Prentice Hall Series in Computational Mathematics (Prentice-Hall, Englewood Cliffs, NJ, 1988).